J. Fluid Mech. (2006), *vol.* 568, *pp.* 203–222.
doi:10.1017/S0022112006002643 Printed in the United Kingdom

Injection of bubbles in a quiescent inviscid liquid under a uniform electric field

By F. J. HIGUERA

E. T. S. Ingenieros Aeronáuticos, UPM, Pza. Cardenal Cisneros 3, 28040 Madrid, Spain

(Received 24 June 2005 and in revised form 27 April 2006)

Numerical computations and order of magnitude estimates are presented for the periodic generation and coalescence of bubbles due to the injection of a constant flow rate of a gas through a circular orifice at the bottom wall of an inviscid dielectric or very polar liquid that is at rest and subject to a uniform vertical electric field far from the orifice. The problem depends on five dimensionless parameters: a Bond number based on the radius of the orifice; Weber and electric Bond numbers whose square roots are dimensionless measures of the flow rate of gas and the applied electric field; the dielectric constant of the liquid; and the contact angle of the liquid with the bottom wall. The bubbles that grow quasi-statically at the orifice for small values of the Weber number are always elongated vertically by the electric stress that acts on their surface when an electric field is applied. The volume of these bubbles at detachment may reach a maximum at a certain value of the electric Bond number, if the Bond number is sufficiently small, or decrease monotonically with the electric Bond number if the Bond number is larger. In both cases the bubbling ceases to be periodic beyond a certain value of the electric Bond number, apparently giving way to more complex bubbling regimes, which are not investigated here. Bubble interaction and eventually coalescence occur when the Weber number is increased keeping the electric Bond number in the range of periodic bubbling. Different periodic regimes are described. It is shown that a moderate electric field may increase the value of the Weber number above which coalescence occurs without changing the shape of the bubbles much. A large electric field may suppress coalescence but it also favours the development of upward and downward jets that cross the bubbles and may cause their breakdown.

1. Introduction

Small bubbles are a common requirement in applications such as bubble-column reactors and boiling heat exchangers, where large rates of heat or mass transfer are sought through an increase in the gas–liquid interface area for a given volume of gas. Other applications of small bubbles include their use as tracers for flow visualization and their use in the fabrication of porous light materials. A high electric field has been often proposed and used as a means of generating small bubbles that can be energetically more efficient than mechanical agitation for liquids of small and moderate electrical conductivity. The reason is that the electric field generates stresses directly at the interface (with a component directed toward the gas) and thus may reduce the waste of mechanical energy in the bulk of the liquid that accompanies mechanical agitation (Tsouris, Shin & Yiacoumi 1998).

Generation of bubbles by injection of a gas into a liquid at rest has been much studied in the absence of an electric field; see Kumar & Kuloor (1970), Clift, Grace &

Weber (1978), Räbiger & Vogelpohl (1986), Tsuge (1986) and Sadhal, Ayyaswamy & Chung (1997) for reviews. At low gas flow rates, the shape of the bubbles growing at the injection orifice is determined by a balance of surface tension and buoyancy forces. The inertia of the liquid begins to have an effect when the flow rate becomes of the order of a certain critical value (reviewed in § 3.3 below), and dominates when the flow rate is further increased, leading to a periodic regime in which the volume of the bubbles increases as the 6/5th power of the gas flow rate and is independent of the surface tension and the size of the orifice (Davidson & Schuler 1960; Ramakrishna, Kumar & Kuloor 1968). This is followed by a sequence of period doubling, involving the interaction and coalescence of successive bubbles and ending in a regime of chaotic bubbling (Tritton & Egdell 1993; Mittoni, Schwarz & La Nauze 1995; Nguyen *et al.* 1996; Tufaile & Sartorelli 2000, 2001).

Zaky & Nossier (1977) observed that the size of the bubbles generated by injecting air into n-heptane and transformer oil through a metallic needle charged to a high voltage relative to a plane electrode immersed in the liquid perpendicularly to the needle decreases when the applied voltage increases. They also measured the increase of the pressure in the bubbles due to the inward electric stress at their surface. In further experiments on the dispersion of bubbles in the non-uniform electric field that exists around an electrified needle, Ogata, Yoshida & Shinohara (1979), Ogata *et al.* (1980) and Ogata *et al.* (1985) investigated the efficiency of this process and the influences of the liquid permittivity and conductivity and of the electrode geometry. Sato, Kuroda & Sakai (1979) and Sato (1980) offered a classification of the bubbling regimes observed when the applied voltage is increased; these range from periodic bubbling to dispersed bubble production and to fine clouds of bubbles at very high voltages. These authors measured the size distribution of bubbles of nitrogen injected into distilled water, showing that it becomes bimodal and develops a long tail at large sizes when the voltage increases. Similar results were obtained by Sato, Saito & Hatori (1993) and Sato, Hatori & Saito (1997) for the electrostatic emulsification of non-conducting liquids of different viscosities in distilled water. Sato *et al.* also proposed that bubble dispersion could be dominated by the electrohydrodynamic flow induced by electric forces acting in the continuous phase.

Tsouris *et al.* (1994, 1995) devised an alternative configuration of the electrodes that is suitable for cases where a non-conducting fluid is injected into a conducting fluid. In their configuration, a large electric field is generated in the inner non-conducting fluid rather than in the outer conducting fluid. This increases the efficiency of the dispersion process by decreasing the electric current and also leads to somewhat smaller bubbles or drops. The effects of the physical properties of the fluids, the geometrical parameters of the nozzle and electrode and the injected flow rate were investigated experimentally by these authors, while Harris & Basaran (1995) carried out numerical computations of the shape and stability of the interface that revealed the influence of the electric stress on surface pinch-off. Shin, Yiacoumi & Tsouris (1997) proposed an empirical model to predict the bubble size as a function of the applied voltage and air flow rate and outlined three different modes of bubble formation: a dripping mode at low voltages and high flow rates; a spraying mode at high voltages and low flow rates; and an erratic mixed mode. Larger flow rates leading to bubble interaction were recently investigated by Sarnobat *et al.* (2004) by injecting nitrogen into glycerol through an electrified needle and applying nonlinear-dynamics analysis tools to their pressure measurements. These authors found period-doubling routes to chaotic bubbling when the electric potential or the flow rate were increased.

Theoretical studies of electrohydrodynamically enhanced boiling heat transfer from a surface heated to a temperature above the boiling temperature of the surrounding liquid were performed by Cheng & Chaddock (1985, 1986) and Ogata & Yabe (1993*a*, *b*). The first authors studied the growth rate and final volume of a bubble attached to a wall in a uniform electric field using a spheroidal approximation for the bubble shape and a simple model for the heat transfer in the boundary layer around the bubble. Ogata and Yabe pointed out the importance of the electric relaxation time of the liquid compared with the characteristic time of bubble development; they accounted for the charge that appears in the bulk of the liquid due to the variation of its electrical conductivity with temperature in the thermal layer around the wall and noticed that the electric force acting on an attached bubble may lead to its horizontal drift on the wall and sometimes also its violent breakup, in addition to vertical elongation of the bubble. Further computations and experimental visualizations of the shape of an attached bubble in uniform and non-uniform electric fields were performed by Cho *et al.* (1996, 1998) and Kweon *et al.* (1998) without any assumptions about the form and magnitude of the surface deformation. Di Marco *et al.* (2003) (see also the references in their paper) investigated experimentally the growth and detachment of bubbles under an electric field in microgravity. A review of the work carried out in the area of heat transfer was given by Seyed-Yagoobi & Bryan (1999).

This paper is devoted to a numerical simulation of the time-periodic generation of bubbles by injection at a constant flow rate of a gas through a circular orifice at the horizontal bottom wall of a liquid which is at rest and subject to a uniform electric field far from the orifice. The liquid will be treated as an inviscid fluid that is either a dielectric or very polar. The assumption of an inviscid liquid has been often used in the analysis of bubble generation in cases when the Reynolds number of the flow induced in the liquid by the expansion of the bubbles growing at the orifice is large; see Oguz & Prosperetti (1993), Oguz & Zeng (1997) and the reviews cited in the second paragraph of this section. At the onset of the high-flow-rate regime, where the inertia of the liquid begins to affect the dynamics of the growing bubbles, this Reynolds number is of order $Re_c = (\gamma a/\rho\nu^2)^{1/2}$ in the absence of an electric field, where ρ, ν and γ are the density, kinematic viscosity and surface tension of the liquid and a is the radius of the injection orifice. Values of Re_c of several hundred are typical of liquids with the physical properties of water and orifice radii of the order of 1 mm, and higher Reynolds numbers are attained when the gas flow rate is further increased or an electric field is applied. The flow of the liquid is irrotational if viscous effects are neglected. In a recent work (Higuera & Medina 2006) it was suggested that the interaction and coalescence of bubbles that occurs in the vicinity of the injection orifice at moderately large values of the gas flow rate can also be analysed with the irrotational-flow approximation. This latter work will be extended here to take into account the presence of an electric field.

The liquid acts as a dielectric when the electric relaxation time, equal to the ratio of the liquid's permittivity to its electrical conductivity, is large compared with the inverse of the bubbling frequency (Saville 1997). In these conditions there is no significant accumulation of free electric charge at the surface of the bubble, and no electric shear stress on this surface, which would be incompatible with the assumption of an irrotational flow. As will be seen in the following section, the analysis of this paper is also valid for very polar liquids irrespective of the value of the electric relaxation time. The reason is that the electric stress on very polar liquids is always nearly perpendicular to their surface, and the electric field becomes independent of the free surface charge. Relaxation times of the order of 1 s or larger can be achieved with

apolar hydrocarbons such as hexane, heptane and cyclohexane, and with refrigerants such as R11 and R113, all of which are less viscous than water and have been used often in the experimental work reviewed above. Since the bubbling periods of these liquids are of the order of 10^{-2} s in the conditions mentioned in the preceding paragraph, they act as dielectrics, to a good approximation, for the bubbling regimes of interest here. Polar liquids of small viscosity are more numerous. However, many of them, including water, have high electrical conductivities, which poses practical problems due to excessive energy dissipation when simple electrode configurations that lead to large electric fields in the liquid are used (Tsouris *et al.* 1994, 1995).

Finally, the limitation of the numerical computations to time-periodic flows sets upper bounds for the gas-flow rate and the electric field, thus leaving out more complex non-periodic and chaotic regimes, whose analysis is not attempted here.

2. Formulation

The following problem is considered. A gas is injected at a constant flow rate through a single circular orifice at the horizontal hydrophilic bottom wall of an inviscid dielectric or very polar liquid that is at rest far from the orifice. A high d.c. voltage is applied between the bottom wall, which is taken to be a perfect conductor, and another horizontal electrode a large distance above the bottom wall. In the absence of gas injection (and assuming that the orifice is covered with a fine metallic grid) this voltage leads to a uniform vertical electric field E_∞ in the liquid. The electric field is distorted when gas is injected through the grid-covered orifice, owing to the difference between the electric permittivity of the gas, ϵ_0, and the electric permittivity of the liquid, $\epsilon_0\epsilon$, where $\epsilon > 1$ is the dielectric constant of the liquid. (See e.g. Wohlhuter & Basaran 1992 and Notz & Basaran 1999 for the better-studied complementary problem of drop injection, for which $\epsilon < 1$).

The electric fields in the liquid and gas phases are of the form $\boldsymbol{E} = \nabla\phi$ and $\boldsymbol{E}^g = \nabla\phi^g$, where ϕ and ϕ^g are the negative of the electric potentials, which are harmonic functions. Hereinafter a superscript g denotes conditions in the gas and the absence of a superscript denotes conditions in the liquid. Assume first that the liquid is a dielectric. Then the boundary conditions for the electric field at the liquid–gas surface are (Landau & Lifshitz 1960)

$$\epsilon E_n = E_n^g \quad \text{and} \quad E_t = E_t^g, \tag{2.1}$$

where the subscripts n and t denote the components of the electric fields normal and tangential to the surface.

In the absence of electric charge in the bulk of the liquid, and assuming that its dielectric constant is uniform, the only effect of the electric field on the motion of the fluids is to produce a stress at the liquid–gas surface that is normal to the surface, points toward the gas and has magnitude (Saville 1997; Landau & Lifshitz 1960)

$$\tau_n^e = \tfrac{1}{2}\epsilon_0\left(E_n^{g^2} - \epsilon E_n^2\right) + \tfrac{1}{2}\epsilon_0(\epsilon - 1)E_t^2. \tag{2.2}$$

Assume now that the liquid has electrical conductivity $K > 0$. Then the electric field leads to a current density $\boldsymbol{j} = K\boldsymbol{E}$, which brings electric charge to the liquid–gas surface. If the electrical conductivity of the gas is neglected, the surface charge density σ satisfies the charge conservation equation (Saville 1997)

$$\frac{\mathrm{D}\sigma}{\mathrm{Dt}} = -K E_n + (\boldsymbol{n}\cdot\nabla\boldsymbol{v}\cdot\boldsymbol{n})\,\sigma. \tag{2.3}$$

Here $\boldsymbol{v}$ is the velocity of the liquid, $\boldsymbol{n}$ is the unit normal to the surface pointing toward the liquid and $\mathrm{D}/\mathrm{D}t = \partial/\partial t + \boldsymbol{v}\cdot\nabla$ is the material derivative at a point on the surface. The two terms on the right-hand side of (2.3) represent the electric charge reaching the surface per unit area per unit time by conduction in the liquid, and the rate of change in σ due to the stretching of the surface.

In the presence of surface charge, the first condition in (2.1) changes to $\epsilon_0(\epsilon E_n - E_n^g) = \sigma$ and an electric shear stress $\tau_t^e = \sigma E_t$ appears at the surface in addition to the normal electric stress (2.2); see Saville (1997). However, accumulation of surface charge to a sufficient level to affect the electric field requires a time of the order of the electric relaxation time $t_e = \epsilon_0\epsilon/K$ (from the order of magnitude balance of the first two terms of (2.3), $\sigma/t_e \sim KE_n$ with $\sigma \sim \epsilon_0\epsilon E_n \sim \epsilon_0 E_n^g$). The effect of the surface charge is therefore negligible, and the liquid can be treated as a perfect dielectric, when the time of growth and detachment of the bubbles is small compared with the electric relaxation time. The effect of the surface charge can be also neglected for very polar liquids ($\epsilon \gg 1$), irrespective of the values of the relaxation and bubbling times. In this limit, the first condition (2.1), or its modified form at the beginning of this paragraph, implies that $E_n \ll E_n^g$, which can be simplified to $E_n = 0$; the expression (2.2) for the normal stress can be simplified to $\tau_n^e = \frac{1}{2}\epsilon_0\epsilon E_t^2$; and the electric shear is small compared with the normal stress, $\tau_t^e/\tau_n = O(1/\epsilon)$, even if $\sigma = O(\epsilon_0 E_n^g)$.

The gas will be treated as an incompressible fluid with a density negligibly small compared with the density of the liquid. The expansion of the bubble growing at the orifice and the rise of the bubbles detached previously induce an irrotational flow in the liquid. The velocity potential, φ such that $\boldsymbol{v} = \nabla\varphi$ in the liquid, the electric potentials in the liquid and in the bubbles, ϕ and ϕ^g, and the surfaces Σ_i of the bubbles (which have equations $f_i(\boldsymbol{x}, t) = 0$ with $f_i > 0$ in the liquid) are determined by the solution of the following problem:

$$\nabla^2\varphi = 0, \quad \nabla^2\phi = 0 \qquad \text{in the liquid;} \tag{2.4}$$

$$\nabla^2\phi^g = 0 \qquad \text{in each bubble;} \tag{2.5}$$

$$\frac{\mathrm{D}f_i}{\mathrm{D}t} = 0, \tag{2.6}$$

$$\frac{\mathrm{D}\varphi}{\mathrm{D}t} = \frac{1}{2}|\nabla\varphi|^2 - p_{g_i} - Bx + \nabla\cdot\boldsymbol{n}_i + \frac{B_E}{2\epsilon}\left\{E_n^{g^2} - \epsilon E_n^2 + (\epsilon - 1)E_t^2\right\} \tag{2.7}$$

and

$$\epsilon E_n = E_n^g, \quad \phi = \phi^g \tag{2.8}$$

at the surface of the ith bubble (the first condition in (2.8) is written here for a dielectric liquid);

$$\frac{\partial\varphi}{\partial x} = 0, \quad \phi = \phi^g = 0 \tag{2.9}$$

at the horizontal bottom wall $x = 0$;

$$\nabla\varphi \to 0, \quad \nabla\phi \to \boldsymbol{e}_x \quad \text{for} \quad \boldsymbol{x} \to \infty; \tag{2.10}$$

and

$$\int_{\Sigma_0} \boldsymbol{v}\cdot\boldsymbol{n}_0\,\mathrm{d}A = We^{1/2}, \qquad \int_{\Sigma_i} \boldsymbol{v}\cdot\boldsymbol{n}_i\,\mathrm{d}A = 0, \quad i = 1, 2, \ldots. \tag{2.11}$$

In these equations x is the vertical distance to the bottom wall, $\boldsymbol{e}_x$ is a unit vector pointing upwards and $\boldsymbol{n}_i = \nabla f_i/|\nabla f_i|$ is the unit normal to the surface of the ith

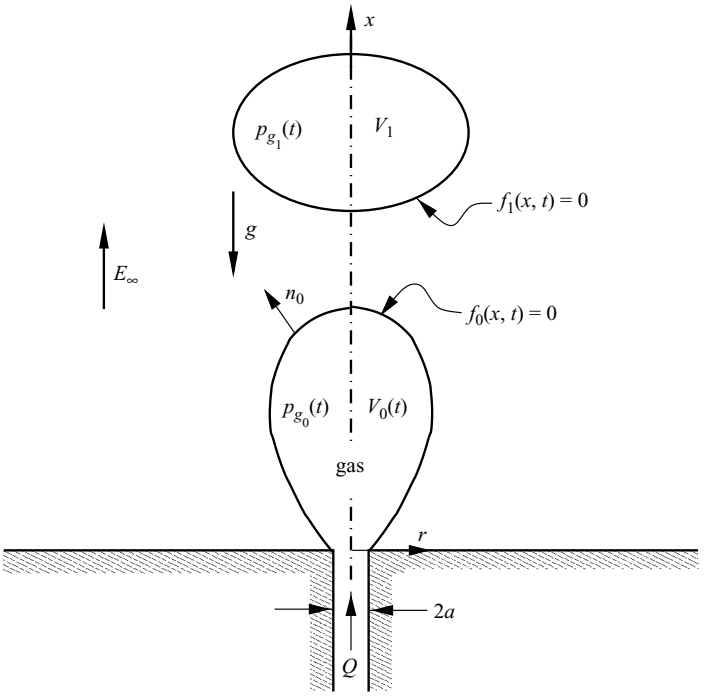

FIGURE 1. Terminology.

bubble, so that $\nabla \cdot \boldsymbol{n}_i$ in (2.7) is the surface tension stress. Here $i = 0$ denotes the bubble attached to the orifice and $i = 1, 2, \ldots$ denote the bubbles detached previously. Distances are scaled with the radius a of the orifice; times are scaled with the capillary time $(\rho a^3/\gamma)^{1/2}$, where ρ and γ are the liquid density and surface tension; the electric potentials are scaled with $E_\infty a$; and $p_{g_i}(t)$ is the pressure of the gas in the ith bubble referred to the pressure of the liquid at the bottom far from the orifice and scaled with γ/a. The dimensionless parameters that appear in the equations are

$$B = \frac{\rho g a^2}{\gamma}, \quad We = \frac{\rho Q^2}{\gamma a^3}, \quad \epsilon, \quad B_E = \frac{\epsilon_0 \epsilon E_\infty^2 a}{\gamma}, \tag{2.12}$$

where g is the acceleration due to gravity and Q is the flow rate of gas injected through the orifice. These parameters are a Bond number, a Weber number, the dielectric constant of the liquid and an electric Bond number, respectively.

Equations (2.11) express the conditions that the volume of the bubble attached to the orifice ($i = 0$) increases at a constant rate equal to the volume of gas injected per unit time ($We^{1/2}$ in dimensionless variables) and that the volumes of the detached bubbles ($i = 1, 2, \ldots$) do not change with time. These equations determine the pressures $p_{g_i}(t)$.

An additional condition is needed at the contact line of the attached bubble and the bottom wall. The condition used here is adopted from Higuera & Medina (2006). A constant contact angle θ is assumed and the contact line is taken to coincide with the edge of the orifice when the angle of the liquid–gas surface with the horizontal is larger than the contact angle (i.e. when $-n_{x_0} < \cos\theta$, where n_{x_0} is the vertical component of the unit normal $\boldsymbol{n}_0$ to the attached bubble, see figure 1) and to shift outward from the orifice, the liquid–gas surface making an angle with the bottom wall equal to the contact angle ($-n_{x_0} = \cos\theta$), otherwise. The contact angle θ is a

fifth parameter of the problem, along with B, We, ϵ and B_E as defined in (2.12). Though the present formulation is valid for any value of θ, numerical results will be given only for liquids that wet the bottom wall with $\theta = 45^\circ$ or smaller. Poor wetting (larger θ) is known to have an effect on the volume of the bubbles generated at small Weber numbers, but this effect will not be discussed here. See Gnyloskurenko *et al.* (2003), Gerlach *et al.* (2005) and Corchero, Medina & Higuera (2006) for recent investigations of the problem of poor wetting in the absence of an electric field.

In the limit of very polar liquids ($\epsilon \to \infty$) the electric stress, within the braces in (2.7), simplifies to $\frac{1}{2}B_E E_t^2$ and the first condition in (2.8) changes to $E_n = 0$. As mentioned earlier, this formulation for very polar liquids is valid even if the electric relaxation time is not large compared to the time of growth and detachment of the bubbles.

Only time-periodic axisymmetric solutions of the problem were computed. This was done numerically by marching in time from an initial state in which gas injection starts without any bubble present in the liquid and letting the system evolve through a number of bubble detachments (and eventually coalescences) until the process becomes periodic to the accuracy of the numerical computations. A standard boundary-element method was used to solve the Laplace equations, and a second-order Runge–Kutta method was used to advance in time the material nodes at the surfaces of the bubbles and the velocity potential at them according to (2.6) and (2.7), $p_{g_i}(t)$ being constrained to satisfy (2.11) at each time step. The numerical method is a straightforward extension of the method used before to compute the injection and coalescence of bubbles in the absence of an electric field (Higuera & Medina 2006), which in turn follows the implementation of Oguz & Prosperetti (1993). Numerical details can be seen in this latter paper and in Oguz & Zeng (1997). See Higuera (2005) for a similar treatment of the moving contact line in the different regime of bubble generation under creeping-flow conditions.

As in the previous work of Higuera & Medina, the number of bubbles simultaneously followed is limited to three by removing the uppermost bubble when a new bubble begins to grow at the orifice. This is a definite approximation, given the elliptic character of the problem. However, tests carried out retaining one more bubble show that the presence of the extra bubble does not drastically change the dynamics of the bubble growing at the orifice and its possible coalescence with the bubble immediately above it. The relative variation in the centre of mass of the most recently detached bubble ($i = 1$) found in these tests was of the order of 5 %, and the observed variations in the shape of the attached bubble and its volume at detachment were smaller than for the bubble $i = 1$. The number of nodes used to discretize the meridian section of the axisymmetric surface of each bubble ranged from 60 to 120 depending on the size of the bubble. Surface reconnections at the detachment of a bubble and at the coalescence of two bubbles were assumed to occur when the distance between the two approaching surfaces becomes smaller than a certain cutoff, which is in the range 0.05 to 0.1 in typical computations. Global results are insensitive to the precise value of the cutoff distance, which is of the order of the separation between the nodes used to discretize the surfaces. It is this separation that determines the accuracy of the entire numerical procedure.

3. Results and discussion

3.1. *Quasi-static bubbles*

Consider first the growth and detachment of bubbles at values of the gas flow rate sufficiently small for the effect of the pressure variations induced in the liquid by the

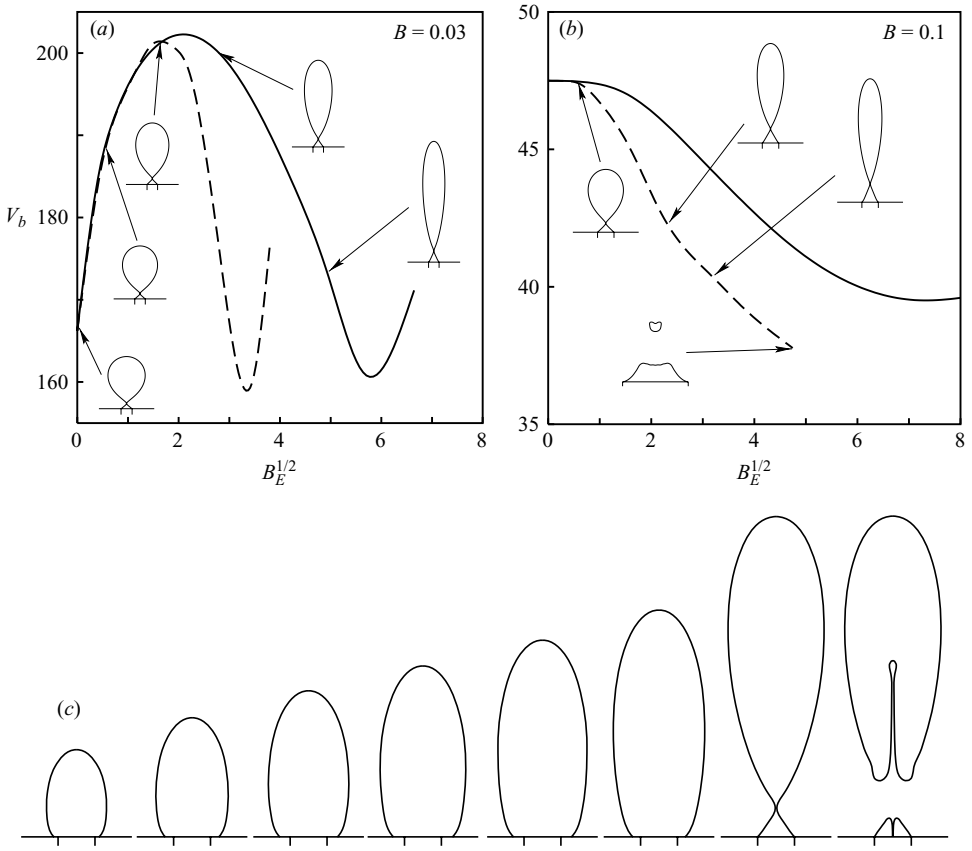

FIGURE 2. Dimensionless volume of the bubbles at detachment (scaled with a^3) as a function of the dimensionless electric field $B_E^{1/2}$ for $\epsilon = 2$ (solid line) and $\epsilon = 10$ (dashed line), at very small values of *We*. (*a*) $B = 0.03$, (*b*) $B = 0.1$. The shapes of the bubbles immediately before detachment are shown for $\epsilon = 2$ in (*a*) and $\epsilon = 10$ in (*b*) at different values of $B_E^{1/2}$; the two small vertical lines in each bubble picture denote the edge of the orifice. (*c*) The shapes of a bubble growing quasi-statically for $B = 0.03$, $B_E^{1/2} = 1.58$, $\epsilon = 10$, $\theta = 45°$, and seven equispaced values of the bubble volume. The rightmost image is not part of the quasi-static evolution. It depicts a rising bubble immediately after detachment and the new bubble left at the orifice, with re-entrant jets in both bubbles.

growth of the bubble attached to the orifice to be small compared with other forces acting on the surface of the bubble. The attached bubble follows then a sequence of quasi-static equilibria with increasing volumes, until detachment occurs when a hydrostatic equilibrium ceases to be possible or becomes unstable. The dimensionless volume of the bubble at detachment is given in figure 2 as a function of the square root of the electric Bond number $B_E^{1/2}$ for different values of ϵ and B. The value $\epsilon = 2$ corresponds to apolar liquids such as cyclohexane or n-heptane, which have been often used in experiments, and $\epsilon = 10$ is representative of polar liquids, for which the electric stress (2.2) is dominated by the term $\frac{1}{2}\epsilon_0\epsilon E_t^2$. The results in figure 2 were obtained from the numerical solution of (2.4)–(2.11) for small values of the Weber number. Different values of *We* in the range 0.05 to 0.5 were used to check the independence of the shape and volume of the bubbles with *We* and thus with the motion of the liquid. The volume of the bubbles does not depend on the precise

value of the contact angle as long as the contact line coincides with the edge of the orifice when the bubble detaches. This condition is satisfied in all the cases displayed in figure 2, which were computed taking $\theta = 45°$, and is also satisfied for any $\theta < 45°$. However, the contact line shifts away from the orifice during part of the quasi-static evolution of the bubble when $B = 0.03$, as illustrated in figure 2(*c*). Larger values of the contact angle or smaller values of B, which would lead to a shift of the contact line that persists at the end of the quasi-static evolution of the attached bubble, were not investigated numerically in the work presented in this paper.

The equilibrium shapes and volumes of the bubbles at detachment were computed by Longuet-Higgins, Kerman & Lunde (1991) in the absence of an electric field. These volumes are thus attained when the electric Bond number $B_E = 0$ in figure 2. The attached bubble becomes increasingly elongated as B_E increases. For small values of the Bond number B, the volume at detachment first increases and then decreases when the electric field increases (figure 2*a*), but the range in which the volume increases disappears at larger values of the Bond number (figure 2*b*). In both cases the volume reaches a minimum at a certain B_E, and the bubbles cease to grow quasi-statically when B_E is increased above the highest values shown in figure 2. Then the meniscus undergoes violent oscillations during the first stages of its growth, its tip sometimes shedding a tiny bubble (as in the lowest inset in figure 2*b*) and sometimes becoming concave and engulting a tiny drop. These results suggest a transition to the spraying or disperse-bubble production regime of Sato (1980) and Shin, Yiacoumi & Tsouris (1997), but such complex regimes cannot be realistically described by axisymmetric computations and will not be discussed in what follows.

Some of the trends shown by the results in figure 2 can be understood in terms of order of magnitude estimates for small values of the Bond number B. These estimates are presented here using dimensional variables. Let us first review the results that exist for $B_E = 0$. It is well known (Davidson & Schuler 1960) that in the absence of an electric field the bubbles growing quasi-statically at the end of a tube or at an orifice in a hydrophilic surface ($\theta \ll 1$) are nearly spherical up to detachment when $B \ll 1$, and their final volume, V_{b_1}, is determined by the balance of the buoyancy force and the surface-tension force acting across the contact line attached to the edge of the orifice:

$$\rho g V_{b_1} = 2\pi\gamma a \tag{3.1}$$

(see Fritz 1935 and Oguz & Prosperetti 1993, for example). This balance gives the Fritz volume $V_{b_1} = 2\pi a\gamma/\rho g$, or $V_{b_1}/a^3 = 2\pi/B$ in dimensionless variables. The bubble is spherical in these conditions because the hydrostatic pressure variation is small compared with the pressure jump due to the surface tension: $(\rho g V_{b_1}^{1/3})/(\gamma/V_{b_1}^{1/3}) = O(B^{1/3}) \ll 1$. Since the surface of the attached bubble is not closed, the gas overpressure, of order $\gamma/V_{b_1}^{1/3}$, gives an upward force of order $a^2\gamma/V_{b_1}^{1/3}$, which should have been included in the balance of forces (3.1) (see Kabanow & Frumkin 1933). This pressure force, however, is smaller than either of the two terms of (3.1) by a factor of order $a/V_{b_1}^{1/3} = O(B^{1/3})$.

When an electric field E_∞ exists far from the attached bubble, an electric stress of order $\epsilon_0\epsilon E_\infty^2$ appears at the surface of the bubble. In the presence of the equipotential bottom wall, this stress gives a downward force of order $\epsilon_0\epsilon E_\infty^2 V_b^{2/3}$ on a bubble of volume V_b, which helps to keep the bubble attached to the orifice. The electric force becomes of the order of the two forces in (3.1) when $B_E = O(B^{2/3})$, where the expression for the Fritz volume V_{b_1} has been used. When $B_E \gg B^{2/3}$ the electric force is large compared with the surface tension force (the right-hand side of (3.1)),

and the volume of the bubble at detachment (V_{b_2} say) is determined to an order of magnitude by the balance $\rho g V_{b_2} \sim \epsilon_0 \epsilon E_\infty^2 V_{b_2}^{2/3}$, which gives $V_{b_2}/a^3 = O(B_E/B)^3$. The predicted increase in the bubble volume with the electric field is displayed by the results of figure 2(*a*) for $B = 0.03$ and moderate values of B_E but not by the results of figure 2(*b*) for $B = 0.1$.

The attached bubble ceases to be spherical (for $B \ll 1$) when the electric stress is able to deform its surface. This happens when $\epsilon_0 \epsilon E_\infty^2 \sim \gamma / V_{b_2}^{1/3}$ or, upon using the estimate of V_{b_2} above, when $B_E = O(B^{1/2})$. The bubble takes then a prolate shape because the inward electric stress is stronger at the equator than at the pole. If the electric field is further increased, the bubble becomes cigar-shaped, with radius $\widetilde{a}$ and height h (at detachment) determined by the order of magnitude balances $\epsilon_0 \epsilon E_\infty^2 \sim \gamma/\widetilde{a} \sim \rho g h$, which give $\widetilde{a}/a = O(1/B_E)$ and $h/a = O(B_E/B)$ in dimensionless variables. The volume of the bubble is now of order $V_{b_3} \sim \widetilde{a}^2 h \sim a^3/(B_E B)$, which decreases with increasing B_E (see figure 2). The electric stress and the surface tension stress $\gamma/\widetilde{a}$ both point toward the gas, increasing its pressure, and their variation with vertical distance balances the hydrostatic depression $\rho g x$ acting on the lateral surface of the bubble. The radius of the bubble $\widetilde{a}$ becomes of the order of the radius of the orifice a when B_E becomes of order unity. This sets an upper bound to the hydrostatic regime in the configuration analysed here, though higher fields may be admissible when the bubble grows by evaporation of the liquid on a surface heated to a temperature above the boiling point of the liquid rather than by injection of gas through an orifice (Cheng & Chaddock 1985, 1986; Ogata & Yabe 1993*a*, *b*).

The estimations in the preceding paragraphs need some changes when the contact angle of the liquid with the bottom wall is not small. Then the radius of the contact line is of the order of the radius of the bubble. The balance of forces (3.1) at detachment in the absence of electric field becomes $\rho g V_b' \sim \gamma V_b'^{1/3}$ in orders of magnitude, giving a modified estimate of the volume $V_{b_1}' \sim (\gamma/\rho g)^{3/2}$, which is independent of a. The electric force begins to matter when $\epsilon_0 \epsilon E_\infty^2 V_{b_1}'^{2/3} \sim \rho g V_{b_1}'$, which amounts to $B_E = O(B^{1/2})$. The results of the preceding paragraph for $B_E \gg B^{1/2}$ are still valid but the surface tension force across the contact line (of characteristic radius $\widetilde{a}$) is now of the order of the electric and buoyancy forces. The intermediate regime $B^{2/3} \ll B_E \ll B^{1/2}$ disappears.

The numerical results of figure 2(*b*) reveal that $B = 0.1$ is not sufficiently small for the bubble volume to display the predicted growth and decay with increasing electric field. To rationalize these results let us decompose the electric stress into a surface-averaged part $\overline{\tau_n^e} = A_b^{-1} \int_{\Sigma_0} \tau_n^e \, \mathrm{d}A$ (where A_b is the area of the attached bubble surface) and a variation about this average $\delta\tau_n^e = \tau_n^e - \overline{\tau_n^e}$. The surface-averaged stress merely increases the pressure of the gas. The vertical force due to $\overline{\tau_n^e}$ would be zero on a closed surface and is downward on the surface of an attached bubble. But this downward force is balanced by the opposite force due to the gas overpressure generated by $\overline{\tau_n^e}$, acting on the horizontal projection of the bubble surface. Thus it is only the vertical force due to $\delta\tau_n^e$ that matters in the balance of forces on the bubble. When it is evaluated from the numerical solutions for $B = 0.1$, this force is upward for small values of B_E (as it would be for a hemispherical bubble, for which an analytic solution exists; see Landau & Lifshitz 1960, pp. 42–43) and decreases and becomes downward when B_E increases, but it is always small compared with the buoyancy and surface tension forces. In these conditions, perhaps the main influence of the electric stresses on the results of figure 2(*b*) is to deform the surface and thus modify the other forces acting on the bubble rather than to impart a vertical force on it directly.

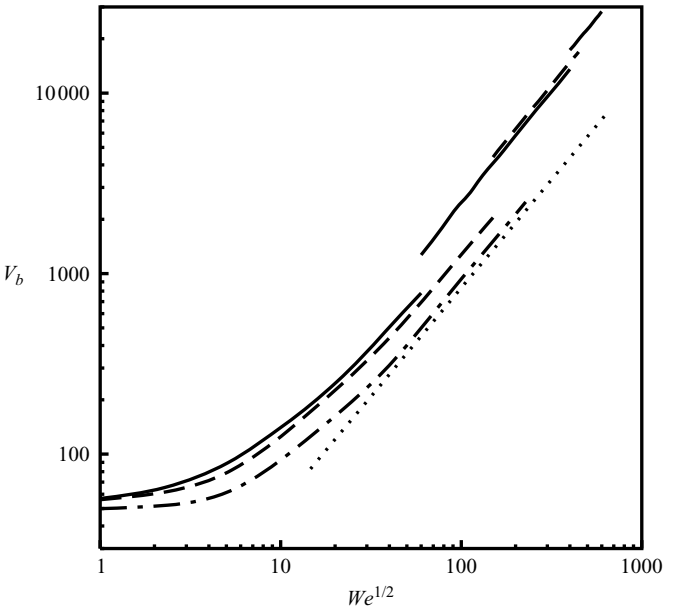

FIGURE 3. Dimensionless volume of the bubbles (scaled with a^3) as a function of the dimensionless flow rate of gas $We^{1/2}$ for $B=0.1$, $\epsilon=10$ and three different values of the electric Bond number. $B_E=0$ (solid curve), 0.9 (dashed curve) and 10 (chain curve). The discontinuities in the first two curves correspond to coalescences of the bubbles. The dotted line at the right-hand side has the slope 6/5 predicted by Davidson & Schuler (1960) for the high-flow-rate regime in the absence of an electric field.

The above decomposition of the electric stresses should be used also for other values of B. However, this formal step is not so important when B is small and the liquid wets the surface, because the force due to $\overline{\tau_n^e}$ is itself negligible when the area of the contact circle is small compared with the area of the bubble.

3.2. *Numerical results for high flow rates*

Figure 3 shows the final volume of the bubbles as a function of the dimensionless flow rate for $B=0.1$, $\epsilon=10$, $\theta=45^\circ$ and three values of the dimensionless electric field. Additional computations carried out for other values of ϵ give results similar to those of figure 3 though, as with the quasi-static solutions of figure 2, the value of the electric field required for the electric stresses to have an effect increases when ϵ is decreased. Similarly, computations carried out elsewhere in the absence of an electric field (Higuera & Medina 2006) show that the process is qualitatively similar for different values of the Bond number B. Finally, the results for high flow rates do not change much when the contact angle is changed. The results of figure 3 are therefore expected to be representative of the solutions for a range of values of B, ϵ and θ.

The discontinuities in the two upper curves of figure 3 (the solid curve, $B_E=0$, and the dashed curve, for which $B_E=0.9$) are due to coalescence of the bubbles upon injection when the Weber number is sufficiently high. In the absence of an electric field, coalescence of bubbles in couples occurs above $We^{1/2}\approx 50$, and the occurrence of two successive coalescences leading to 'triple bubbles' begins for $We^{1/2}$ slightly above 400. When an electric field is applied, coalescences are postponed to higher values of the Weber number. Only single coalescences are observed in the numerical results for $B_E=0.9$, when $We^{1/2}$ is higher than about 150, and no coalescence is observed for

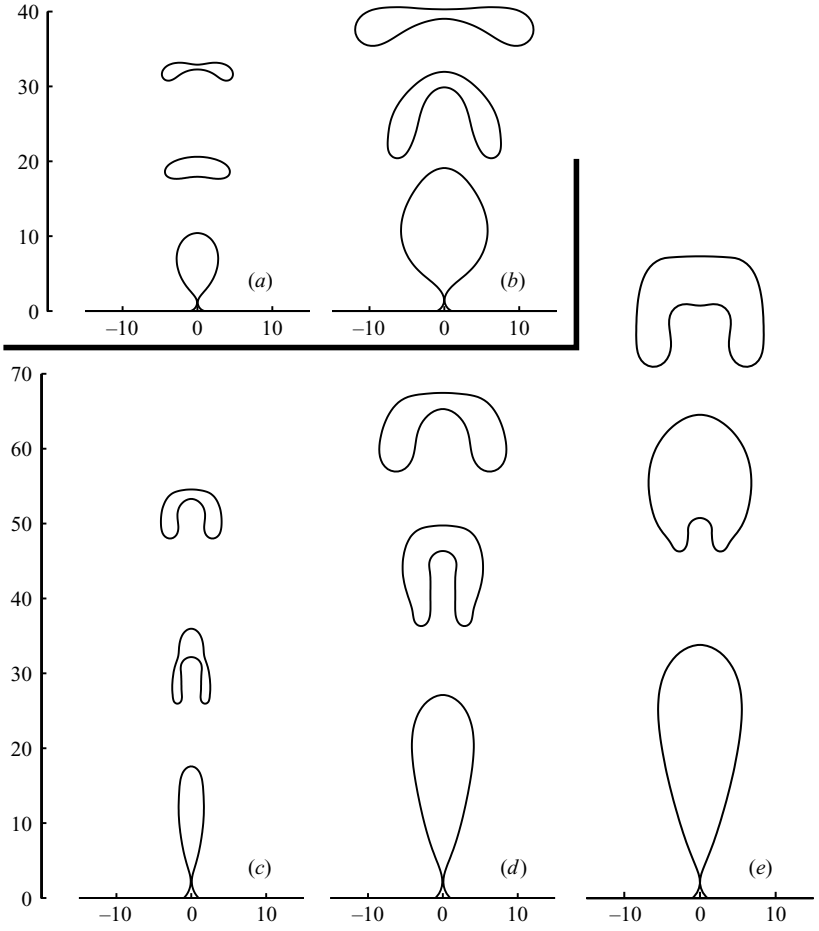

FIGURE 4. Periodic generation of single bubbles for $B = 0.1$, $\epsilon = 10$ and various values of B_E and We. (*a*) $B_E = 0.9$, $We^{1/2} = 10$ (period = 12.51); (*b*) $B_E = 0.9$, $We^{1/2} = 80$ (period = 12.20); (*c*) $B_E = 10$, $We^{1/2} = 10$ (period = 9.28); (*d*) $B_E = 10$, $We^{1/2} = 80$ (period = 8.88); (*e*) $B_E = 10$, $We^{1/2} = 150$ (period = 10.06). The pattern at the instant of detachment of a bubble is shown in each case.

$B_E = 10$ (the chain curve in figure 3). This is probably the most important effect of the electric field in the range of flow rates explored here.

Solutions for different values of B_E and $We^{1/2}$ before the onset of coalescence are compared in figures 4(*a–d*). The shapes of the bubbles in the upper row of the figure, for $B_E = 0.9$, are not much affected by the electric stress. The mean distance between bubbles decreases, and their mutual interaction therefore increases, when the Weber number increases. The bubbles in (*c*) and (*d*) of the lower row, for $B_E = 10$ and the same two values of the Weber number as in (*a*) and (*b*), are much more elongated by the electric stress while they are attached to the orifice. The shape of these bubbles changes much upon detachment, and during a certain lapse of time they rise faster than the rounder bubbles of (*a*) and (*b*), which increases their spacing and inhibits their coalescence in the vicinity of the orifice (cf. estimates in § 3.3 below). Case (*e*) of figure 4, for $B_E = 10$ and $We^{1/2} = 150$, has no analogue in the upper row because the bubbles already coalesce at this Weber number when $B_E = 0.9$.

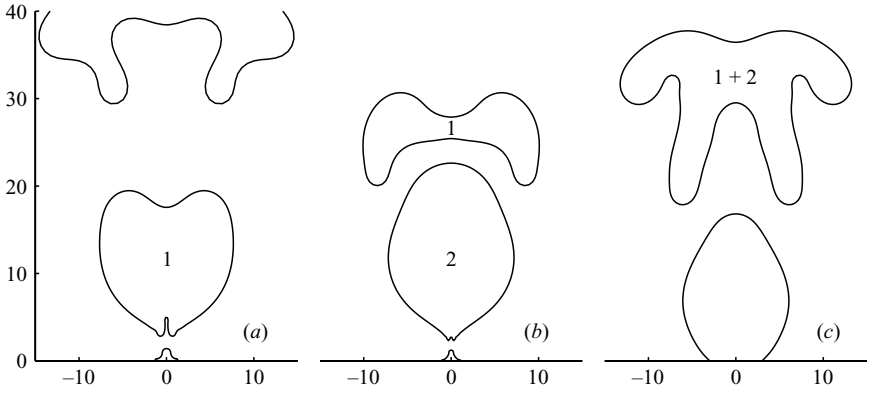

FIGURE 5. The generation of a compound bubble for $B = 0.1$, $\epsilon = 10$, $B_E = 0.9$ and $We^{1/2} = 150$. (*a*) $t = 14.06$, immediately after the detachment of the leading bubble; (*b*) $t = 24.88$, immediately after the detachment of the trailing bubble; (*c*) $t = 33.05$, immediately after coalescence of the two bubbles. Times are non-dimensionalized with the capillary time $(\rho a^3/\sigma)^{1/2}$ and measured from the time of detachment of the bubble preceding bubble 1 in (*a*). The period of the process is 24.88. Notice the displacement of the contact line away from the orifice in (*c*).

The coalescence of bubbles in couples for $B_E = 0.9$ and $We^{1/2} = 150$ is illustrated in figure 5. The leading bubble of each couple (labelled 1 in the figure) grows and detaches. The trailing bubble (labelled 2) grows in the presence of the first bubble, detaches from the orifice, rises faster than the leading bubble and coalesces with it at a certain height above the orifice to form the bubble $1 + 2$. This regime of bubbling is well documented in the absence of an electric field and was termed the pairing regime by Zhang & Shoji (2001). The present computations show that a moderate electric field ($B_E = 0.9$) postpones the pairing regime to higher values of the Weber number without changing it qualitatively, while a high electric field ($B_E = 10$) suppresses the pairing regime.

The height of coalescence decreases when the Weber number is increased while keeping the other parameters constant. Detachment of the trailing bubble and coalescence are almost simultaneous events for a range of Weber numbers, and the trailing bubble coalescences with the leading bubble before detaching from the orifice when the Weber number is further increased. Then the sequence detachment–detachment–coalescence changes to detachment–coalescence–detachment. This latter sequence is illustrated in the upper row of figure 6 for $B_E = 0$ and $We^{1/2} = 400$. The lower row of figure 6, for $B_E = 0.9$ and $We^{1/2} = 400$, still displays the former sequence, though detachment of the trailing bubble, in 6(*e*), occurs only slightly before coalescence, in 6(*f*).

The lower part of the surface of a detached bubble is often concave toward the liquid. The origin of this concavity is in the retraction of the surface immediately after pinch-off, which leads to a re-entrant jet at the base of the most recently detached bubble (Räbiger & Vogelpohl 1986). The tip of this jet may break and give birth to one or a few small drops that shoot across the bubble and hit the upper part of the surface, as in figure 6(*c*); see Higuera & Medina (2006) for a discussion of this phenomenon and comparisons with experimental visualizations. The upper part of the surface of an attached bubble may also become concave, and sometimes a downward moving jet that enters the orifice develops in this region, a phenomenon known as weeping (Zhang & Tan 2000). In the presence of an electric field, the electric stresses favour the growth of any concavity once it is formed, and thus a concavity in the upper part of an attached bubble may persist after the bubble detaches. This can be

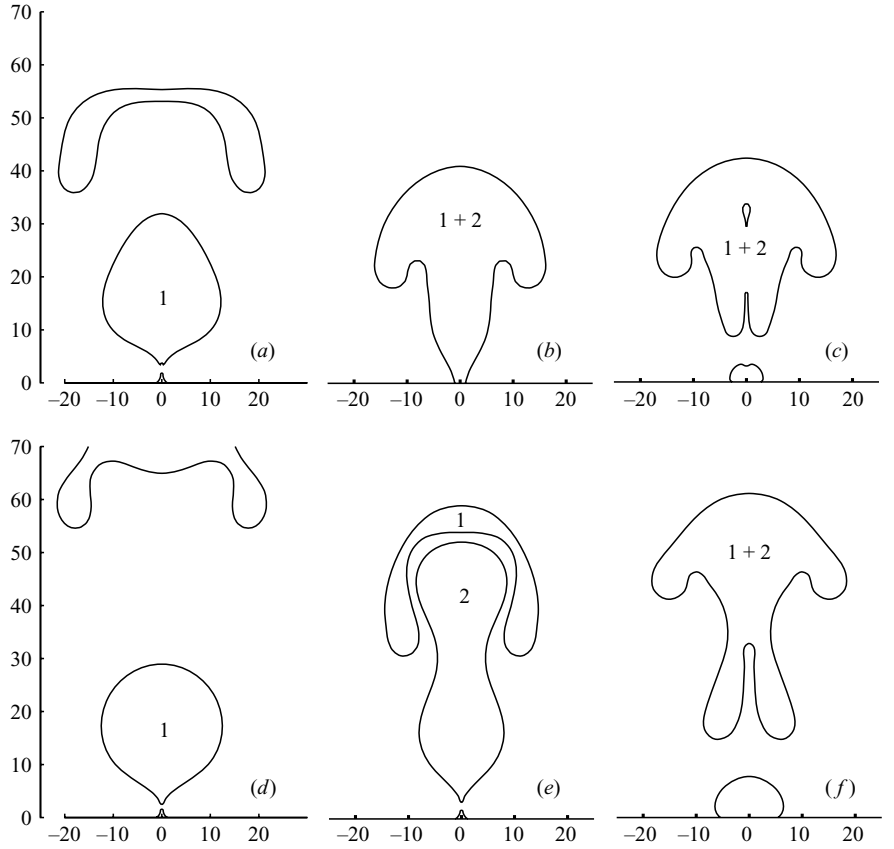

FIGURE 6. Upper row: The generation of a compound bubble for $B = 0.1$, $B_E = 0$ and $We^{1/2} = 400$. (*a*) $t = 18.49$, immediately after the detachment of the leading bubble; (*b*) $t = 30.79$, immediately after coalescence of the leading (detached) and trailing (attached) bubbles; (*c*) $t = 31.75$, immediately after detachment of the double bubble (the contact line is displaced away from the orifice). The period of the process is 31.56. Lower row: The same process for $B = 0.1$, $\epsilon = 10$, $B_E = 0.9$ and $We^{1/2} = 400$. (*d*) $t = 18.89$, immediately after the detachment of the leading bubble; (*e*) $t = 33.85$, immediately after the detachment of the trailing bubble; (*f*) $t = 35.64$, immediately after coalescence of the two bubbles (the contact line is displaced away from the orifice). The period of the process is 33.85. Non-dimensional times are measured from the detachment of the bubble preceding bubble 1.

seen in bubbles 1 and 1 + 2 of figure 5. At high Weber numbers the concavities tend to develop into upward or downward moving jets that may pierce the bubbles and transform them into tori. Since toroidal bubbles are very unstable to non-axisymmetric perturbations and rapidly break down (Räbiger & Vogelpohl 1986), piercing has been taken to define an upper bound for the Weber number beyond which axisymmetric solutions are not realistic (Higuera & Medina 2006). The presence of an electric field lowers this upper bound (see figure 3). The bubbles attached to the orifice undergo extensive weeping for $B_E = 10$ and values of $We^{1/2}$ higher than about 200 (which may cast some doubts on the validity of the assumption of axisymmetry even at these early stages of the bubble evolution). These bubbles detach with a volume considerably higher than the volume obtained by extrapolation of the chain curve of figure 3 and become toroidal bubbles a short time after detachment.

3.3. *Order of magnitude estimates for* $B \ll 1$

The order of magnitude estimates of § 3.1 are extended here to larger values of the Weber number. As before, dimensional variables are used and the known results for $B_E = 0$ are reviewed first.

3.3.1. *High-flow-rate regime of periodic bubbling in the absence of an electric field*

Davidson & Schuler (1960) and Ramakrishna, Kumar & Kuloor (1968) showed that a high-flow-rate inertia-dominated regime of periodic bubbling exists in which, in the absence of an electric field, the effect of the surface tension is negligible and the volume of the bubbles increases as the 6/5th power of the flow rate. In this regime the velocity of order $v_e = O(Q/V_b^{2/3})$ induced in the liquid by the expansion of an attached bubble of volume V_b leads to pressure variations of order ρv_e^2, which exert a downward force of order $\rho v_e^2 V_b^{2/3}$ on the surface of the bubble. This force is now large compared with the surface tension force acting across the contact line and is the force that buoyancy has to overcome in order to detach the bubble. The order of magnitude balance $\rho g V_b \sim \rho(Q/V_b^{2/3})^2 V_b^{2/3}$ gives the bubble volume estimated by Davidson & Schuler (1960) and Ramakrishna, Kumar & Kuloor (1968) for the high-flow-rate regime as $V_b \sim V_{b_4} = Q^{6/5}/g^{3/5}$ or, in dimensionless terms, $V_{b_4}/a^3 = (We/B)^{3/5}$.

The transition from the quasi-static regime of § 3.1 to the high-flow-rate regime discussed above occurs when the surface tension, buoyancy and flow-induced pressure forces are all of the same order. When the contact angle is small and the contact line coincides with the edge of the orifice, this condition reads $\gamma a \sim \rho g V_b \sim \rho v_e^2 V_b^{2/3}$ (or, equivalently, $V_{b_1} \sim V_{b_4}$), which is satisfied for $We \sim We_{c_1} = 1/B^{2/3}$. When the contact angle is not small and the radius of the contact line is of order $V_b^{1/3}$ rather than a, the transition ($V'_{b_1} \sim V_{b_4}$) occurs for $We \sim We'_{c_1} = 1/B^{3/2}$.

It is worth noticing that, in the case of $\theta \ll 1$, surface tension forces keep the attached bubble spherical in the high-flow-rate regime when $\rho v_e^2 \ll \gamma/V_{b_4}^{1/3}$, which amounts to $We \ll 1/B^{3/2}$. These are Weber numbers much larger than We_{c_1}, when B is small.

3.3.2. *High-flow-rate regime in the presence of an electric field*

The estimates of the previous subsection are applicable in the presence of an electric field if the electric force is small compared with the buoyancy force, which is the case for $B_E \ll B^{2/3}$ when the contact angle is small and for $B_E \ll B^{1/2}$ otherwise (cf. § 3.1). If these conditions are not satisfied then the transition from the quasi-static regime to the high-flow-rate regime occurs when the flow-induced pressure force becomes of the order of the buoyancy and electric forces.

Consider first the transition when the electric Bond number is in the range $B^{2/3} \ll B_E \ll B^{1/2}$, which is relevant for small contact angles. Surface tension keeps the quasi-static bubble spherical in this range of B_E, and the balances defining the onset of the high-flow-rate regime read $\rho v_e^2 V_b^{2/3} \sim \epsilon_0 \epsilon E_\infty^2 V_b^{2/3} \sim \rho g V_b$, which amount to $V_{b_2} \sim V_{b_4}$ and give $We \sim We_{c_2} = B_E^5/B^4$. Surface tension still keeps the bubble spherical in the high-flow-rate regime when $We_{c_2} \ll We \ll 1/B^{3/2}$.

Consider now the onset of the high-flow-rate regime for $B_E \gg B^{1/2}$, which corresponds to cigar-shaped bubbles in the quasi-static regime of § 3.1. When the finite growth rate of the bubble is taken into account, its lateral expansion induces a horizontal velocity $v_e = O(Q/(h\tilde{a}))$ in the surrounding liquid. The counterpressure of the liquid on the surface is thus of order $\rho v_e^2 \sim \rho(Q^2/a^4)B^2$, where the quasi-static estimates of $\tilde{a}$ and h worked out in § 3.1 have been used. This counterpressure

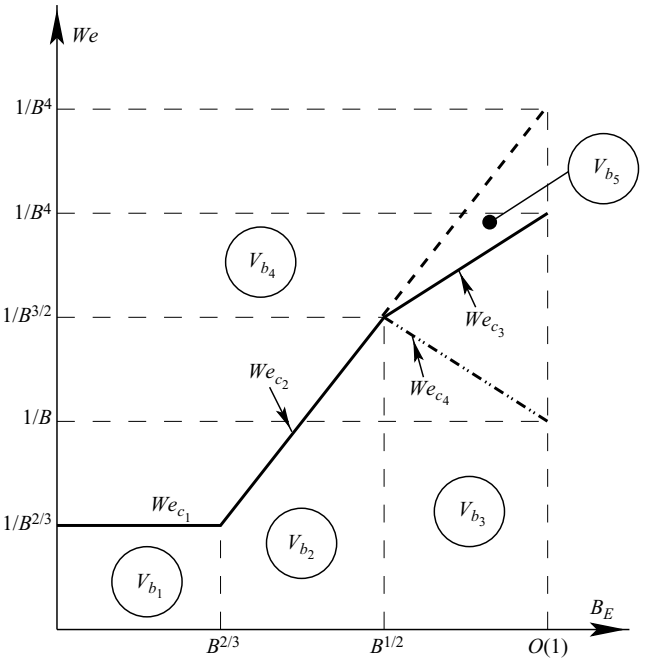

FIGURE 7. Sketch of the solution regimes for $B \ll 1$ and a hydrophilic bottom surface. The solid line We_{c_1}–We_{c_2}–We_{c_3} gives the upper bound of the quasi-static regime for different ranges of B_E. Bubble interaction occurs above this line and above the chain line at the right. The order of magnitude of the volume of the bubbles at detachment is indicated in the different regions.

becomes of the order of the electric stress ($\rho v_e^2 \sim \epsilon_0 \epsilon E_\infty^2$) when $We \sim We_{c_3} = B_E/B^2$, which defines the onset of the high-flow-rate regime for $B_E \gg B^{1/2}$.

If $We \gg We_{c_3}$ (and $B_E \gg B^{1/2}$) then the normal stress due to the surface tension becomes negligible and the conditions determining the radius $\widetilde{a}$ and height h of the bubble at detachment in the high-flow-rate regime are $\rho(Q/h\widetilde{a})^2 \sim \epsilon_0 \epsilon E_\infty^2 \sim \rho g h$, which give $\widetilde{a}/a \sim We^{1/2} B/B_E^{3/2}$ and $h/a \sim B_E/B$. The volume of the bubble is now of order $V_{b_5} \sim \widetilde{a}^2 h \sim a^3 We B/B_E^2$, which increases linearly with We (rather than with the classic 3/5th power law) and decreases with increasing B_E. The condition $h \gg \widetilde{a}$ requires that $We \ll We_{c_2}$. Cigar-shaped bubbles occur in the high-flow-rate regime within the range $We_{c_3} \ll We \ll We_{c_2}$, where the effect of the electric field is to decrease the volume of the bubbles: $V_{b_5}/V_{b_4} \sim (We/We_{c_2})^{2/5} \ll 1$. The electric stresses cease to play an important role and the bubble becomes round with a volume of order V_{b_4} when $We \gg We_{c_2}$.

The estimates of this section and of § 3.1 are schematically summarized in figure 7 for the case of a hydrophilic surface ($\theta \ll 1$). The case of non-small contact angles is simpler, in that the two lines $We = We_{c_1}$ and $We = We_{c_2}$ of figure 7 defining the upper bound of the quasi-static regime for $B_E \ll B^{1/2}$ are replaced by the single horizontal line $We = We'_{c_1} = 1/B^{3/2}$.

3.3.3. *Interaction and coalescence of bubbles*

The possibility of the interaction and coalescence of successive bubbles upon injection (in the vicinity of the orifice) depends on the ratio of the time of growth of a bubble attached to the orifice and the time it takes for a recently detached bubble to rise to a height above the orifice of the order of the size of the bubble. The time

of growth is $t_{growth} = V_b/Q$, where V_b is the volume of the bubble at detachment. The time of rise depends on the apparent mass of the bubble.

The apparent mass of the round bubbles that obtain for $B_E \ll B^{1/2}$ is of order ρV_b, and the time of rise to a height $V_b^{1/3}$ is of order $t_{rise} = V_b^{1/6}/g^{1/2}$. The ratio $t_{rise}/t_{growth} = Q/(g^{1/2}V_b^{5/6})$ can be evaluated using the various estimates of V_b worked out before. In the quasi-static regime it is $V_b \sim V'_{b_1}$ when the contact angle is not small, and $V_b \sim V_{b_1}$ for $B_E \ll B^{2/3}$ or $V_b \sim V_{b_2}$ for $B^{2/3} \ll B_E \ll B^{1/2}$ when the contact angle is small. This gives $t_{rise}/t_{growth} \sim (We/We'_{c_1})^{1/2}$ in the first case, $t_{rise}/t_{growth} \sim (We/We_{c_1})^{1/2}$ in the second case and $t_{rise}/t_{growth} \sim (We/We_{c_2})^{1/2}$ in the third case. All these time ratios are small, implying that the interaction between bubbles is negligible in the quasi-static regime. In the high-flow-rate regime, however, the bubble volume is $V_b \sim V_{b_4}$ and $t_{rise}/t_{growth} \sim 1$, so that bubble interaction and coalescence should be expected. Since $We_{c_2} \gg We_{c_1}$ (see figure 7), the effect of an electric field satisfying $B^{2/3} \ll B_E \ll B^{1/2}$ is to postpone bubble interaction for small contact angles to values of the gas flow rate higher than in the absence of the field. The price to be paid is an increase in the volume at detachment, because $V_{b_2} > V_{b_1}$.

The estimate of t_{rise} must be modified for the elongated bubbles that appear when $B_E \gg B^{1/2}$. The apparent mass of an elongated bubble of radius $\tilde{a}$ and height h is of order $\rho\tilde{a}^3$, and the distance it has to travel to move out of the region where the following bubble grows is of order h. Now the acceleration–buoyancy balance $\rho\tilde{a}^3(h/t_{rise}^2) \sim \rho g V_b$ (with $V_b \sim \tilde{a}^2 h$) gives $t_{rise} \sim (\tilde{a}/g)^{1/2}$ and thus $t_{rise}/t_{growth} \sim Q/(g^{1/2}\tilde{a}^{3/2}h)$. This ratio is small only if $We \ll We_{c_4} = 1/(B_E B)$, which is small compared with We_{c_3}. At variance with this estimation, the numerical results of figure 3 show that the electric field inhibits the coalescence of elongated bubbles. The explanation is probably in the change in shape of the bubbles upon detachment mentioned in § 3.2.

4. Conclusions

The periodic bubbling of a gas that is fed at a constant flow rate through an orifice at the bottom wall of a liquid at rest has been investigated numerically when the liquid is subject to an electric field due to a high d.c. voltage applied between the horizontal bottom wall and another horizontal electrode at a large distance above the bottom wall. An inviscid liquid is assumed that is either a dielectric or very polar. In the absence of space charge in the bulk of the liquid and space variations of its dielectric constant, the only effect of the electric field is to generate a stress at the liquid–gas surface that is normal to the surface and directed toward the gas. The problem depends on five dimensionless parameters.

The bubbles grow quasi-statically at the injection orifice when the Weber number based on the flow rate of gas is small. The electric stresses elongate the quasi-static bubbles vertically and affect their volume at detachment. This volume may either decrease when the electric field is increased or first increase and then decrease. In both cases the numerical results show that a properly chosen electric field can reduce the volume of the bubbles. The orderly quasi-static growth of the attached bubbles comes to an end when the electric field is increased above a certain value, apparently giving way to more complex regimes of bubbling (not discussed here) in which tiny bubbles and drops are shed by an attached meniscus.

The pressure variations due to the flow induced in the liquid by the expansion of an attached bubble begin to affect the bubble when the Weber number becomes

of the order of a certain critical value that marks the transition to a high-flow-rate regime in which the interaction and eventually coalescence of bubbles occur in the vicinity of the injection orifice. A moderate electric field is found to increase the Weber number at which coalescence begins, thus decreasing the final volume of the generated bubbles. This effect is more pronounced when the electric field is increased, but high fields also favour the development of strong vertical jets that cross the bubbles and may cause their breakdown. Estimates of the Weber number of transition to the high-flow-rate regime as a function of the electric Bond number have been worked out in the asymptotic limit of small Bond numbers.

This work was supported by the Spanish Ministerio de Educación y Ciencia under projects DPI2002–4550–C07-05 and DPI2004–05246–C04–02, and by UPM–CM project R05/9961.

REFERENCES

Cheng, K. J. & Chaddock, J. B. 1985 Effect of and electric field on bubble growth rate. *Intl Comm. Heat Mass Transfer* **12**, 259.

Cheng, K. J. & Chaddock, J. B. 1986 Maximum size of bubbles during nucleate boiling in an electric field. *Intl J. Heat Mass Transfer* **7**, 278.

Cho, H. J., Kang, I. S., Kweon, Y. C. & Kim, M. H. 1996 Study of the behavior of a bubble attached to a wall in a uniform electric field. *Intl J. Multiphase Flow* **22**, 909.

Cho, H. J., Kang, I. S., Kweon, Y. C. & Kim, M. H. 1998 Numerical study of the behavior of a bubble attached to a tip in a nonuniform electric field. *Intl J. Multiphase Flow* **24**, 479.

Clift, R., Grace, J. R. & Weber, M. E. 1978 *Bubbles, Drops, and Particles*. Academic.

Corchero, G., Medina, A. & Higuera, F. J. 2006 Effects of wetting conditions and flow rate on bubble formation at orifices submerged in water. *J. Colloids Surfaces* A (to appear, available on line).

Davidson, J. F. & Schuler, B. O. G. 1960 Bubble formation at an orifice in an inviscid liquid. *Trans. Inst. Chem. Engrs* **38**, 335.

Di Marco, P., Grassi, W., Memoli, G., Takamasa, T., Tomiyama, A. & Hosokawa, S. 2003 Influence of electric field on single gas-bubble growth and detachment in microgravity. *Intl J. Multiphase Flow* **29**, 559.

Fritz, W. 1935 Berechnung des maximalen Volumens von Dampfblasen. *Phys. Z.* **36**, 379.

Gerlach, D., Biswas, G., Durst, F. & Kolobaric, V. 2005 Quasi-static bubble formation on submerged orifices. *Intl J. Heat Mass Transfer* **48**, 425.

Gnyloskurenko, S., Byakova, A., Raychenko, O. & Nakamura, T. 2003 Influence of wetting conditions on bubble formation at orifice in an inviscid liquid. Transformation of bubble shape and size. *Colloids Surf.* A **218**, 73.

Harris, M. T. & Basaran, O. A. 1995 Equilibrium shapes and stability of nonconducting pendant drops surrounded by a conducting fluid in an electric field. *J. Colloid Interf. Sci.* **170**, 308.

Higuera, F. J. 2005 Injection and coalescence of bubbles in a very viscous liquid. *J. Fluid Mech.* **530**, 369.

Higuera, F. J. & Medina, A. 2006 Injection and coalescence of bubbles in a quiescent inviscid liquid. *Eur. J. Mech./*B **25**, 164.

Kabanow, B. & Frumkin, A. 1933 Über die Grösse elektrolytisch entwickelter Gasblasen. *Z. Physik. Chem.* A **165**, 433.

Kumar, R. & Kuloor, N. R. 1970 The formation of bubbles and drops. *Adv. Chem. Engng* **8**, 255.

Kweon, Y. C., Kim, M. H., Cho, H. J. & Kang, I. S. 1998 Study of the deformation and departure of a bubble attached to a wall in d.c/a.c electric fields. *Intl J. Multiphase Flow* **24**, 145.

Landau, L. D. & Lifshitz, E. M. 1960 *Electrodynamics of Continuous Media*. Pergamon.

Longuet-Higgins, M. S., Kerman, B. R. & Lunde, K. 1991 The release of air bubbles from an underwater nozzle. *J. Fluid Mech.* **230**, 365.

Mittoni, L. J., Schwarz, M. P. & La Nauze, R. D. 1995 Deterministic chaos in the gas inlet pressure of gas-liquid bubbling systems. *Phys. Fluids* **7**, 891.

Nguyen, K., Daw, C. S., Chakka, P., Cheng, M., Bruns, D. D. & Finney, C. E. A. 1996. Spatio-temporal dynamics of a train of rising bubbles. *Chem. Engng Sci.* **65**, 191.

Notz, P. K. & Basaran, O. A. 1999 Dynamics of drop formation in an electric field. *J. Colloid Interface Sci.* **213**, 218.

Ogata, J. & Yabe, A. 1993*a* Basic study on the enhancement of nucleate boiling heat transfer by applying electric fields. *Intl J. Heat Mass Transfer* **36**, 775.

Ogata, J. & Yabe, A. 1993*b* Augmentation of boiling heat transfer by utilizing the EHD effect–EHD behavior of boiling bubbles and heat transfer characteristics. *Intl J. Heat Mass Transfer* **36**, 783.

Ogata, S., Shigehara, K., Yoshida, T. & Shinohara, H. 1980 Small air bubble formation by using strong nonuniform electric field. *IEEE Trans. IAS* **16**, 766.

Ogata, S., Tan, K., Nishijima, K. & Chang, J.-S. 1985 Development of improved bubble disruption and dispersion technique by an applied electric field method. *AIChE J.* **31**, 62.

Ogata, S., Yoshida, T. & Shinohara, H. 1979 Small air bubble formation in insulating liquids under strong nonuniform electric field. *Japan J. Appl. Phys.* **18**, 411.

Oguz, H. N. & Prosperetti, A. 1993 Dynamics of bubble growth and detachment from a needle. *J. Fluid Mech.* **257**, 111.

Oguz, H. N. & Zeng, J. 1997 Axisymmetric and three-dimensional boundary integral simulations of bubble growth from an underwater orifice. *Engng Anal. Boundary Elements* **19**, 319.

Räbiger, N. & Vogelpohl, A. 1986 Bubble formation and its movement in newtonian and non-newtonian liquids. In *Encyclopedia of Fluid Mechanics*, Vol. 3 (ed. N. P. Cheremisinoff), chap. 4. Gulf.

Ramakrishna, S., Kumar, R. & Kuloor, N. R. 1968 Studies in bubble formation–I: Bubble formation under constant flow conditions. *Chem. Engng Sci.* **24**, 731.

Sadhal, S. S., Ayyaswamy, P. S. & Chung, J. N. 1997 *Transport Phenomena with Drops and Bubbles*, Chap. 7. Springer.

Sarnobat, S. U., Rajput, S., Bruns, D. D., DePaoli, D. W., Daw, C. S. & Nguyen, K. 2004 The impact of external electrostatic fields on gas-liquid bubbling dynamics. *Chem. Engng Sci.* **59**, 247.

Sato, M. 1980 Cloudy bubble formation in a strong nonuniform electric field. *J. Electrostatics* **8**, 285.

Sato, M., Hatori, T. & Saito, M. 1997 Experimental investigation of droplet formation mechanisms by electrostatic dispersion in a liquid-liquid system. *IEEE Trans.* IA **33**, 1527.

Sato, M, Kuroda, M. & Sakai, T. 1979 Effect of electrostatics on bubble formation. *Kagaku Kogaku Ronbunshu* **5**, 380.

Sato, M., Saito, M. & Hatori, T. 1993 Emulsification and size control of insulating and/or viscous liquids in liquid-liquid systems by electrostatic dispersion. *J. Colloid Interface Sci.* **156**, 504.

Saville, D. A. 1997 Electrohydrodynamics: The Taylor-Melcher leaky dielectric model. *Annu. Rev. Fluid Mech.* **29**, 27.

Seyed-Yagoobi, J. & Bryan, J. E. 1999 Enhancement of heat transfer and mass transport in single-phase and two-phase flows with electrohydrodynamics. *Adv. Heat Transfer* **33**, 95.

Shin, W.-T., Yiacoumi, S. & Tsouris, C. 1997 Experiments on electrostatic dispersion of air into water. *Ind. Engng Chem. Res.* **36**, 3647.

Tritton, D. J. & Egdell, C. 1993 Chaotic bubbling. *Phys. Fluids* A **5**, 503.

Tsouris, C., DePaoli, D. W., Feng, J. Q., Basaran, O. A. & Scott, T. C. 1994 Electrostatic spraying of nonconductive fluids into conductive fluids. *AIChE J.* **40**, 1920.

Tsouris, C., DePaoli, D. W., Feng, J. Q., Basaran, O. A. & Scott, T. C. 1995 Experimental investigation of electrostatic dispersion of nonconductive fluids into conductive fluids. *Ind. Engng Chem. Res.* **34**, 1394.

Tsouris, C., Shin, W.-T. & Yiacoumi, S. 1998 Pumping, spraying, and mixing of fluids by electric fields. *Can. J. Chem. Engng* **76**, 589.

Tsuge, H. 1986 Hydrodynamics of bubble formation from submerged orifices. In *Encyclopedia of Fluid Mechanics*, Vol. 3 (ed. N. P. Cheremisinoff), chap. 9. Gulf.

Tufaile, A. & Sartorelli, J. C. 2000 Chaotic behavior in bubble formation dynamics. *Physica* A **275**, 336.

Tufaile, A. & Sartorelli, J. C. 2001 The circle map dynamics in air bubble formation. *Phys. Lett.* A **287**, 74.

Wohlhuter, F. K. & Basaran, O. A. 1992 Shapes and stability of pendant and sessile drops in an electric field. *J. Fluid Mech.* **235**, 481.

Zaky, A. A. & Nossier, A. 1977 Bubble injection and electrically induced hydrostatic pressure in insulating liquids subjected to non-uniform fields. *J. Phys.* D: *Appl. Phys.* **10**, L189.

Zhang, L. & Shoji, M. 2001 Aperiodic bubble formation from a submerged orifice. *Chem. Engng Sci.* **56**, 5371.

Zhang, W. & Tan, R. B. H. 2000 A model for bubble formation and weeping at a submerged orifice. *Chem. Engng Sci.* **55**, 6243.